Modeling of an Unmanned Hybrid Aerial Vehicle

Guillaume Ducard, Minh Duc Hua

Accepted version of the paper : G. Ducard, M.-D Hua, "Modeling of an Unmanned Hybrid Aerial Vehicle," Proceedings of the IEEE Multi-conference on Systems and Control (MSC), Invited session on UAVs, pp. 1011 – 1016, Antibes, France, 8-10 October 2014. https://doi.org/10.1109/CCA.2014.6981467

Modeling of an Unmanned Hybrid Aerial Vehicle

Guillaume Ducard[1] and Minh-Duc Hua[2]

***Abstract*— In this paper, the mathematical modeling of a hybrid aerial vehicle is presented. This vehicle is a combination of a fixed-wing aircraft and a multirotor helicopter. This vehicle is thus capable of vertical take off and landing (VTOL) and of cruising forward flight. The thrust is generated by 4 propellers which can pivot and thus the direction of thrust is controllable. This paper details the nonlinear dynamics of the aircraft, including major aerodynamics effects and thrust-tilting effects, resulting in a realistic simulator for control design and validation.**

I. INTRODUCTION

Unmanned aerial vehicles (UAVs) have become very popular for military and civil applications, but also for academic research. These vehicles belong to either the rotary-wing or the fixed-wing categories. In the first category, like standard helicopters, weight is compensated by the thrust induced by the propellers. In the second category, like standard airplanes weight is compensated by the lift force induced by the air flux on the wing(s) resulting from the vehicle's airspeed. The main advantage of rotary-wing vehicles is their ability to take-off vertically and perform hovering, which is very useful for many inspection and surveillance applications and when confined environment requires to take-off vertically. A limitation of rotary-wing vehicles, however, is their modest energy efficiency compared to conventional aircrafts. In the last few years, there has been an increased interest in a third category of vehicles, which tries to combine advantages of both rotary-wing and fixed-wing vehicles. These so-called "convertible UAVs" are typically composed of propellers allowing for vertical take-off and wings for energy efficiency in cruising flight [5], [12], [1], [7].

In this paper, a novel "convertible" design constructed by Wingcopter is presented, which is a combination of a fixed-wing aircraft and a quadrotor helicopter. In addition, the thrust generated by the 4 propellers can be rotated two-by-two simultaneously and, thus, the thrust direction can be monitored. This tilting mechanism is different from the one of twin-rotors [6] or other tilting multi-rotors [9], [3], [2], and constitutes the major novelty of this design. This paper aims at modeling the most relevant nonlinear dynamics, including major aerodynamics effects and thrust-tilting effects, resulting in a realistic simulator for control design and validation.

[1]Guillaume Ducard is with Univ. Nice Sophia Antipolis, CNRS, I3S, UMR 7271, 06900 Sophia Antipolis, France. ducard@i3s.unice.fr

[2]Minh-Duc Hua is with ISIR, CNRS-UPMC, Paris, France. hua@isir.upmc.fr

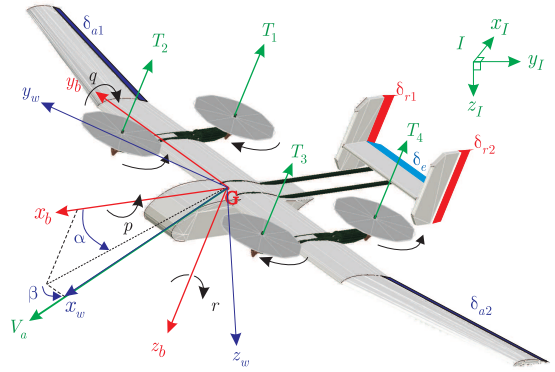

Fig. 1. Wingcopter, coordinates systems and some notations

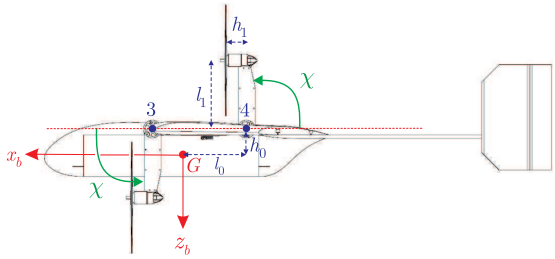

Fig. 2. Wingcopter side view, with propellers tilted by an angle $\chi = \frac{\pi}{2}$

II. VEHICLE DESCRIPTION AND DYNAMICS

The vehicle is sketched in Figs. 1 and 2. This hybrid flying machine is designed on the basis of a fixed-wing aircraft. On each wing, a pair of propellers is mounted with a mechanism that enables to tilt simultaneously the propellers of one pair around the y_b axis by an angle $\chi \in [0, \pi/2]$, as shown in Fig. 2. The angle corresponding to the right (resp. left) pair of propellers is denoted χ_R (resp. χ_L). Therefore, it is possible to control the direction of the total thrust generated by the 4 propellers about the y_b axis. In addition, alike classical quadrotor UAVs, it is also possible to monitor the control torque vector by controlling the 4 propellers' speed, in addition to aerodynamic torques from control surfaces. The vehicle is equipped with 4 control surfaces, namely an aileron on each wing with a deflection δ_{a1} and δ_{a2}, respectively, an elevator with a deflection δ_e, and two rudders with deflection angles δ_{r1} and δ_{r2}, respectively. The airspeed vector V_a makes an angle β with the plane (x_b, z_b), which is also known as the sideslip angle. The angle of attack is α as shown in Fig. 1.

A. Attitude Representation

Let $\mathcal{I} = \{0; x_I, y_I, z_I\}$ denotes an inertial frame with z_I pointing downward, which is consistent with the common use of NED (North-East-Down) frames in aeronautics. Let $\mathcal{B} = \{G; x_b, y_b, z_b\}$ denotes a body frame, with G the vehicle's center of mass. The orientation of the aircraft body-fixed frame $\mathcal{B}$ with respect to the inertial frame $\mathcal{I}$ can be represented by a rotation matrix $\boldsymbol{R}_{\mathcal{I}}^{\mathcal{B}}$, which can also be related to a quaternion representation $\boldsymbol{q}_{\mathcal{I}}^{\mathcal{B}} = [q_0, \boldsymbol{q}_v]^\top$ using the Rodrigues' rotation formula: $\boldsymbol{R}_{\mathcal{I}}^{\mathcal{B}} = \boldsymbol{I}_3 + 2q_0\boldsymbol{q}_{v\times} + 2(\boldsymbol{q}_{v\times})^2$, with $\boldsymbol{I}_3$ the 3×3 identity matrix, and $(\cdot)_\times$ denoting the skew-symmetric matrix associated with the cross product, i.e. $\boldsymbol{u}_\times \boldsymbol{v} = \boldsymbol{u}_\times \boldsymbol{v}$, $\forall \boldsymbol{u}, \boldsymbol{v} \in \mathbb{R}^3$.

B. Dynamics of the Center of Gravity

The differential equations of the nonlinear six degree-of-freedom aircraft model are summarized as below. First, the position vector $\boldsymbol{p}$ between a reference point in the inertial frame (attached to ground) and the center of mass G of the aircraft, has the coordinates $\boldsymbol{p}^{\mathcal{I}}$ in the inertial frame, and the coordinates $\boldsymbol{p}^{\mathcal{B}}$ in the aircraft body-fixed frame. The relationship between these coordinates is $\boldsymbol{p}^{\mathcal{I}} = \boldsymbol{R}_{\mathcal{B}}^{\mathcal{I}} \boldsymbol{p}^{\mathcal{B}}$. Second, the coordinates of the inertial velocity vector are $\dot{\boldsymbol{p}}^{\mathcal{I}}$, and in the body frame they are $\dot{\boldsymbol{p}}^{\mathcal{B}}$, with the relationship $\dot{\boldsymbol{p}}^{\mathcal{I}} = \boldsymbol{R}_{\mathcal{B}}^{\mathcal{I}} \dot{\boldsymbol{p}}^{\mathcal{B}}$. The vehicle dynamics in the body frame are expressed as: $\ddot{\boldsymbol{p}}^{\mathcal{B}} = -\boldsymbol{\omega} \times \dot{\boldsymbol{p}}^{\mathcal{B}} + g\boldsymbol{R}_{\mathcal{I}}^{\mathcal{B}} \boldsymbol{e_3} + \frac{1}{m}\left(\boldsymbol{F}_r^{\mathcal{B}} + \boldsymbol{F}_a^{\mathcal{B}}\right)$, with m the vehicle's mass, $\boldsymbol{e_3} = [0\ 0\ 1]^\top$, $\boldsymbol{F}_r^{\mathcal{B}}$ the total force induced by the 4 propellers/rotors systems, $\boldsymbol{F}_a^{\mathcal{B}}$ the total aerodynamic forces, and $\boldsymbol{\omega} := \boldsymbol{\omega}_{\mathcal{B}/\mathcal{I}}^{\mathcal{B}} = [p, q, r]^\top$ the body-rotation rates vector.

C. Attitude Dynamics

The attitude of the aircraft is described by either

1) the direction cosine matrix $\boldsymbol{R}_{\mathcal{I}}^{\mathcal{B}}$, whose dynamics are $\dot{\boldsymbol{R}}_{\mathcal{B}}^{\mathcal{I}} = \boldsymbol{R}_{\mathcal{B}}^{\mathcal{I}} \boldsymbol{\omega}_\times$.
2) or the quaternion $\boldsymbol{q}_{\mathcal{I}}^{\mathcal{B}}$, whose dynamics are given by

$$\dot{\boldsymbol{q}}_{\mathcal{I}}^{\mathcal{B}} = \frac{1}{2}\begin{bmatrix} 0 & -\boldsymbol{\omega}^\top \\ \boldsymbol{\omega} & -\boldsymbol{\omega}_\times \end{bmatrix} \boldsymbol{q}_{\mathcal{I}}^{\mathcal{B}}.$$

D. Turn-rates Dynamics

The dynamics of the aircraft turn-rates, expressed in the body frame, are as follows:

$$\boldsymbol{I}^{\mathcal{B}} \dot{\boldsymbol{\omega}} = -\boldsymbol{\omega}_\times \boldsymbol{I}^{\mathcal{B}} \boldsymbol{\omega} + \boldsymbol{\Gamma}_r^{\mathcal{B}} + \boldsymbol{\Gamma}_a^{\mathcal{B}} \tag{1}$$

with $\boldsymbol{I}^{\mathcal{B}}$ the vehicle's inertial matrix, $\boldsymbol{\Gamma}_r^{\mathcal{B}}$ the total torque generated by the 4 propellers/rotors systems, and $\boldsymbol{\Gamma}_a^{\mathcal{B}}$ the total aerodynamic torque.

III. Tilting Mechanism and Propellers/Rotors Systems

A. Propeller Forces and torques modelling for simulation

Each propeller $i = 1, \cdots, 4$ generates a thrust force vector expressed in the body frame

$$\boldsymbol{T}_i^{\mathcal{B}} = T_i \boldsymbol{u}_i^{\mathcal{B}} = -T_i \mathbf{R}_{\chi_i} \mathbf{e}_3 = T_i \begin{bmatrix} \sin\chi_i \\ 0 \\ -\cos\chi_i \end{bmatrix} \tag{2}$$

with the rotor-tilting angle χ_i belonging to the range $[0, \frac{\pi}{2}]$ and increasing when turning about the axis $(-\boldsymbol{y}_b)$ and

$$\boldsymbol{R}_{\chi_i} = \begin{bmatrix} \cos\chi_i & 0 & -\sin\chi_i \\ 0 & 1 & 0 \\ \sin\chi_i & 0 & \cos\chi_i \end{bmatrix}$$

One notes that $\chi_1 = \chi_2 = \chi_R$ and $\chi_3 = \chi_4 = \chi_L$.

The relative position of the four rotors' center with respect to the vehicle's CoM, expressed in the body frame, are given by $\boldsymbol{d}_{ri}^{\mathcal{B}} = \boldsymbol{d}_i + \boldsymbol{R}_{\chi_i} \boldsymbol{d}_{ei}, \quad i = 1, \cdots, 4$ with

$$\begin{aligned} \boldsymbol{d}_1 &= \begin{bmatrix} -l_0 & L_0 & -h_0 \end{bmatrix}^\top, & \boldsymbol{d}_{e1} &= \begin{bmatrix} -l_1 & 0 & -h_1 \end{bmatrix}^\top \\ \boldsymbol{d}_2 &= \begin{bmatrix} l_0 & L_0 & -h_0 \end{bmatrix}^\top, & \boldsymbol{d}_{e2} &= \begin{bmatrix} l_1 & 0 & -h_1 \end{bmatrix}^\top \\ \boldsymbol{d}_3 &= \begin{bmatrix} l_0 & -L_0 & -h_0 \end{bmatrix}^\top, & \boldsymbol{d}_{e3} &= \begin{bmatrix} l_1 & 0 & -h_1 \end{bmatrix}^\top \\ \boldsymbol{d}_4 &= \begin{bmatrix} -l_0 & -L_0 & -h_0 \end{bmatrix}^\top, & \boldsymbol{d}_{e4} &= \begin{bmatrix} -l_1 & 0 & -h_1 \end{bmatrix}^\top \end{aligned}$$

Then, the position of the i-th rotor's center, expressed in the inertial frame, satisfies $\boldsymbol{p}_{ri}^{\mathcal{I}} = \boldsymbol{p}^{\mathcal{I}} + \boldsymbol{R}_{\mathcal{B}}^{\mathcal{I}} \boldsymbol{d}_{ri}^{\mathcal{B}}, \quad i = 1, \cdots, 4$ the differentiation of which yields

$$\dot{\boldsymbol{p}}_{ri}^{\mathcal{I}} = \dot{\boldsymbol{p}}^{\mathcal{I}} + \boldsymbol{R}_{\mathcal{B}}^{\mathcal{I}} \boldsymbol{\omega}_\times \boldsymbol{d}_i + \boldsymbol{R}_{\mathcal{B}}^{\mathcal{I}} (\boldsymbol{\omega} + \dot{\chi}_i \boldsymbol{e}_2)_\times \boldsymbol{R}_{\chi_i} \boldsymbol{d}_{ei}$$

As a consequence, one can verify that the velocity of the i-th rotor's center, expressed in the i-th rotor frame, is given by

$$\boldsymbol{v}_{ri} = \boldsymbol{R}_{\chi_i}^\top (\dot{\boldsymbol{p}}^{\mathcal{B}} + \boldsymbol{\omega}_\times \boldsymbol{d}_i) + \boldsymbol{R}_{\chi_i}^\top (\boldsymbol{\omega} + \dot{\chi}_i \boldsymbol{e}_2)_\times \boldsymbol{R}_{\chi_i} \boldsymbol{d}_{ei} \tag{3}$$

From here, the freestream velocity acting on the i-th rotor, expressed in the i-th rotor frame, can be computed as

$$\boldsymbol{v}_{ai} = \boldsymbol{R}_{\chi_i}^\top \boldsymbol{R}_{\mathcal{I}}^{\mathcal{B}} \boldsymbol{v}_w^{\mathcal{I}} - \boldsymbol{v}_{ri} \tag{4}$$

with $\boldsymbol{v}_w^{\mathcal{I}}$ the wind velocity expressed in the inertial frame.

We continue to compute the thrust intensity T_i and the induced velocity v_{ri}^{ind} for the i-th rotor. The well-known Glauert's formula yields the following relation between v_{ri}^{ind} and the thrust intensity T_i of the rotor:

$$v_{ri}^{ind} \sqrt{(v_{ai,1})^2 + (v_{ai,2})^2 + (v_{ai,3} + v_{ri}^{ind})^2} = \frac{T_i}{2\rho A} \tag{5}$$

with ρ the air density, $A = \pi R^2$ the rotor's area, and R the propeller radius. We assume that the rotor speed is high w.r.t. the freestream velocity ($\varpi \in [3000; 6000] RPM$ at normal operating conditions) so that the reverse flow region can be neglected and the angle of attack of the blade remains small.Based on classical blade element theory, the thrust intensity can be proximately obtained as follows (see, e.g., [4, Ch.5],[7])

$$T_i \approx c_T \left(1 + \frac{3}{2}\bar{\nu}_{1,2}^2 - a_T \bar{\nu}_{3,ind}\right) \varpi_i^2 \tag{6}$$

with $\bar{\nu}_{1,2} := \frac{\sqrt{(v_{ai,1})^2 + (v_{ai,2})^2}}{\varpi_i R}$, $\bar{\nu}_{3,ind} := \frac{v_{ai,3} + v_{ri}^{ind}}{\varpi_i R}$, and c_T and a_T some constant parameters which depend on the geometry of the propeller. Then, Eqs. (5) and (6) can be used to solve (numerically) the two unknown variables T_i and v_{ri}^{ind}. In the present study, we further simplify Eq. (6) by neglecting the term v_{ri}^{ind}, yielding

$$T_i \approx c_T \left(1 + \frac{3}{2}\bar{\nu}_{1,2}^2 - a_T \frac{v_{ai,3}}{\varpi_i R}\right) \varpi_i^2 \tag{7}$$

with ϖ_i the speed of the i-th rotor. With T_i now (approximately) known, one can solve Eq. (5) to obtain the induced velocity v_{ri}^{ind} using, for example, the Newton-Raphson numerical method with the initial condition $v_{ri}^{ind} = \sqrt{\frac{T_i}{2\rho A}}$.

The resisting torque $\boldsymbol{Q}_{ri}^{\mathcal{B}}$ and the induced drag $\boldsymbol{D}_{ind,ri}^{\mathcal{B}}$ acting on the i-th rotor, expressed in the body frame, can be approximately given by (see, e.g., [4, Ch.5],[7])

$$\boldsymbol{Q}_{ri}^{\mathcal{B}} \approx \lambda_i c_Q \left(1 + \bar{\nu}_{1,2}^2 + a_Q \bar{\nu}_{3,ind}\right) \varpi_i^2 \boldsymbol{u}_i^{\mathcal{B}} \tag{8}$$

$$\boldsymbol{D}_{ind,ri}^{\mathcal{B}} \approx \frac{2c_Q}{R^2}\left(1 + \frac{3a_Q}{4}\bar{\nu}_{3,ind}\right) \varpi_i \boldsymbol{R}_{\chi_i} \begin{bmatrix} v_{ai,1} \\ v_{ai,2} \\ 0 \end{bmatrix} \tag{9}$$

with c_Q and a_Q some constant parameters dependent on the geometry of the propeller, $\lambda_1 = \lambda_3 = 1$, $\lambda_2 = \lambda_4 = -1$.

Gyroscopic effects due to the rotation of the propellers and the rotor-tilting motion are also important to be modeled. Assume that for each mobile arm the inertia is mainly due to the propeller/rotor group. The angular velocity of the i-th propeller expressed in the body frame is

$$\boldsymbol{\omega}_{ri}^{\mathcal{B}} = \lambda_i \varpi_i \boldsymbol{u}_i^{\mathcal{B}} - \dot{\chi}_i \mathbf{e}_2 \approx \lambda_i \varpi_i \boldsymbol{u}_i^{\mathcal{B}}$$

where the latter approximation is justified by the fact that $\dot{\chi}_i \ll \varpi_i$. Then, the gyroscopic precession torque of the i-th propeller is approximately given by

$$\boldsymbol{\Gamma}_{G,ri}^{\mathcal{B}} \approx \lambda_i \varpi_i I_P \boldsymbol{u}_i^{\mathcal{B}} \times \boldsymbol{\omega} \tag{10}$$

with the scalar I_P the inertia of the propeller/rotor group about the rotor axis.

Finally, the total force and torque, expressed in the body frame, due to the four propeller/rotor groups are given by

$$\begin{aligned} \boldsymbol{F}_r^{\mathcal{B}} &= \textstyle\sum_i \left(T_i \mathbf{u}_i^{\mathcal{B}} + \boldsymbol{D}_{ind,ri}^{\mathcal{B}}\right) \\ \boldsymbol{\Gamma}_r^{\mathcal{B}} &= \textstyle\sum_i \left(\boldsymbol{Q}_{ri}^{\mathcal{B}} + \boldsymbol{\Gamma}_{G,ri}^{\mathcal{B}} + \boldsymbol{d}_{ri}^{\mathcal{B}} \times (\mathbf{T}_i^{\mathcal{B}} + \boldsymbol{D}_{ind,ri}^{\mathcal{B}})\right) \end{aligned} \tag{11}$$

B. Simplified model for control allocation Near Hover

The control allocation considered in this section is the following: "Given a desired thrust intensity T and control torque $\boldsymbol{\Gamma_c} \in \mathbb{R}^"$, determine the rotors' speed ϖ_i". This control allocation problem is mainly used when the vehicle is near hovering, with χ_R and χ_L small (*i.e.,* fuselage and wing horizontal) in which case the control surfaces are less efficient.

Assume, for instance, that the left and right tilting-arms rotate with the same angle, i.e. $\chi_L = \chi_R = \chi$. In this case, all the four rotors tilt in the same direction, that is $\mathbf{u}_i^{\mathcal{B}} = \mathbf{u}^{\mathcal{B}} = \begin{bmatrix}\sin\chi & 0 & -\cos\chi\end{bmatrix}^\top = -\mathbf{R}_\chi \mathbf{e}_3$, for all $i \in \{1,2,3,4\}$. The expressions of T_i and $\boldsymbol{Q}_{ri}^{\mathcal{B}}$, given by Eqs. (7) and (8), are further simplified as follows

$$T_i = c_T \varpi_i^2, \ \boldsymbol{Q}_{ri}^{\mathcal{B}} = \lambda_i c_Q \varpi_i^2 \mathbf{u}^{\mathcal{B}} \tag{12}$$

As a consequence, the total control thrust intensity can be deduced as $T = c_T \sum_i \varpi_i^2$, and the total control torque vector verifies

$$\begin{aligned} \boldsymbol{\Gamma_c} &= c_Q \sum_i \lambda_i \varpi_i^2 \mathbf{u}^{\mathcal{B}} + \sum_i \lambda_i c_T \varpi_i^2 \boldsymbol{d}_{ri}^{\mathcal{B}} \times \mathbf{u}^{\mathcal{B}} \\ \Rightarrow \mathbf{R}_\chi^\top \boldsymbol{\Gamma_c} &= -\sum_i \lambda_i c_Q \varpi_i^2 \mathbf{e}_3 \\ &\quad - \sum_i c_T \varpi_i^2 ((\mathbf{R}_\chi^\top \boldsymbol{d}_i) \times \mathbf{e}_3 + \boldsymbol{d}_{ei} \times \mathbf{e}_3) \end{aligned}$$

One then deduces then following relation between the rotors' speed ϖ_i and the vector composed of T and $\mathbf{R}_\chi^\top \boldsymbol{\Gamma_c}$:

$$\begin{bmatrix} T \\ \mathbf{R}_\chi^\top \boldsymbol{\Gamma_c} \end{bmatrix} = \mathbf{A}_c \begin{bmatrix} \varpi_1^2 & \varpi_2^2 & \varpi_3^2 & \varpi_4^2 \end{bmatrix}^\top \tag{13}$$

with the allocation matrix

$$\mathbf{A}_c = \begin{bmatrix} c_T & c_T & c_T & c_T \\ -L_0 c_T & -L_0 c_T & L_0 c_T & L_0 c_T \\ a_{31} & a_{32} & a_{33} & a_{34} \\ -c_Q & c_Q & -c_Q & c_Q \end{bmatrix}$$

with the terms $a_{31} = a_{34} = (-l_1 - l_0 \cos\chi - h_0 \sin\chi) c_T$ and the terms $a_{32} = a_{33} = (l_1 + l_0 \cos\chi - h_0 \sin\chi) c_T$. One verifies that $\det(\mathbf{A}_c) = -16 c_Q c_T^3 L_0 (l_0 + l_1 \cos\chi) \neq 0$, which implies that $\mathbf{A}_c$ is invertible. Thus, T and $\boldsymbol{\Gamma_c}$ can be given any desired values –modulo the constraint of positivity of ϖ_i^2 and the limited range of velocities imposed by power limitations of the rotors.

C. Propeller Rate Model

The propeller rate dynamics are modeled as a first order system with time constant τ_n, which corresponds to the dynamics of a brushless motor as used on the Wingcopter :

$$\dot{\varpi}_i = -\frac{1}{\tau_n}\varpi_i + \frac{1}{\tau_n}\varpi_c \ . \tag{14}$$

IV. AERODYNAMIC FORCES: $\boldsymbol{F_a}^{\mathcal{B}}$

The air flow acting on the airframe is responsible for the aerodynamic forces. The air flow is described by the airspeed vector $\boldsymbol{V_a}$. Its norm is V_a and its direction relative to the airframe is defined by two angles, namely the angle of attack α and the sideslip angle β.

As shown in Fig. 1, the angle of attack α is the angle between the projection of the airspeed vector $\boldsymbol{V_a}$ onto the (x_b, z_b) plane and the x_b axis. The sideslip angle β is the angle between the projection of the airspeed vector $\boldsymbol{V_a}$ onto the (x_b, z_b) plane and the airspeed vector itself. The wind axes coordinate system is such that the x_w axis points along the airspeed vector $\boldsymbol{V_a}$.

The rotation matrix $\boldsymbol{R}_{\mathcal{B}}^{\mathcal{W}}$ is necessary to transform vectors and point coordinates from the aircraft body-fixed frame ($\mathcal{B}$) to the wind frame ($\mathcal{W}$) and *vice versa* according to the following formulae:

$$\boldsymbol{A}^{\mathcal{W}} = \boldsymbol{R}_{\mathcal{B}}^{\mathcal{W}} \boldsymbol{A}^{\mathcal{B}} \qquad \text{or} \qquad \boldsymbol{A}^{\mathcal{B}} = (\boldsymbol{R}_{\mathcal{B}}^{\mathcal{W}})^T \boldsymbol{A}^{\mathcal{W}} = \boldsymbol{R}_{\mathcal{W}}^{\mathcal{B}} \boldsymbol{A}^{\mathcal{W}}$$

with

$$\boldsymbol{R}_{\mathcal{B}}^{\mathcal{W}} = \begin{bmatrix} \cos\alpha\cos\beta & \sin\beta & \sin\alpha\cos\beta \\ -\sin\beta\cos\alpha & \cos\beta & -\sin\alpha\sin\beta \\ -\sin\alpha & 0 & \cos\alpha \end{bmatrix} .$$

As an example, the airspeed vector is expressed in the body-fixed frame as $\boldsymbol{V}_a^{\mathcal{B}} = \boldsymbol{R}_{\mathcal{W}}^{\mathcal{B}} \boldsymbol{V}_a^{\mathcal{W}}$ or as follows:

$$\begin{bmatrix} u_a & v_a & w_a \end{bmatrix}^\top = \boldsymbol{R}_{\mathcal{W}}^{\mathcal{B}} \begin{bmatrix} V_a & 0 & 0 \end{bmatrix}^\top .$$

The subscript $()_a$ is used to distinguish the coordinates of the airspeed vector $\boldsymbol{V}_a^{\mathcal{B}}$ from the coordinates of the aircraft's inertial velocity vector $\boldsymbol{v}^{\mathcal{B}} = [u \quad v \quad w]^\top$.

A. Wind Effects

The aircraft's inertial velocity $\boldsymbol{v}$ is the sum of the airspeed $\boldsymbol{V_a}$ and the wind velocity $\boldsymbol{v}_w$, $\boldsymbol{v} = \boldsymbol{V_a} + \boldsymbol{v}_w$.

For a wind disturbance given by its coordinates in the inertial frame $\boldsymbol{v}_w^{\mathcal{I}}$, the airspeed vector in body frame is given by $\boldsymbol{V}_a^{\mathcal{B}} = \boldsymbol{v}^{\mathcal{B}} - \boldsymbol{R}_{\mathcal{I}}^{\mathcal{B}} \boldsymbol{v}_w^{\mathcal{I}}$. For the nonlinear simulations of the aircraft, the aerodynamic forces and torques are functions of the angle of attack α, the sideslip angle β, the airspeed V_a, and the dynamic pressure $\bar{q}$. They are defined as follows:

$$V_a = \sqrt{u_a^2 + v_a^2 + w_a^2}\,, \; \alpha = \arctan\left(\frac{w_a}{u_a}\right), \quad (15)$$

$$\beta = \arcsin\left(\frac{v_a}{V_a}\right), \; \bar{q} = \frac{\rho V_a^2}{2} . \quad (16)$$

There are several aerodynamic forces acting on this vehicle. The aerodynamic forces $\boldsymbol{F}_a$ acting on a surface in relative motion with the air are composed of the lift force $\boldsymbol{F}_L$ and the drag force $\boldsymbol{F}_D$ as $\boldsymbol{F}_a = \boldsymbol{F}_D + \boldsymbol{F}_L$. When the aerodynamic forces are projected in the body frame, they are decomposed as follows:

$$\boldsymbol{F}_a^{\mathcal{B}} = \begin{pmatrix} X^{\mathcal{B}} & Y^{\mathcal{B}} & Z^{\mathcal{B}} \end{pmatrix}^\top = \boldsymbol{R}_{\mathcal{W}}^{\mathcal{B}} \begin{pmatrix} X^{\mathcal{W}} & Y^{\mathcal{W}} & Z^{\mathcal{W}} \end{pmatrix}^\top$$

B. The Wing

The objective of this section is to model and characterize the behavior of the wing, in terms of lift and drag forces, over a large range of the angle of attack since this type of vehicle is capable of vertical-wing flight, as well as horizontal-wing flight. However, we consider that the sideslip angle β remains rather small, *i.e.* within the range $[-20, +20]$, which is a reasonable assumption since the vehicle is equipped with a vertical tail naturally aligning the airframe with the airflow. When aerodynamics forces and moments are concerned, a key aerodynamic parameter to consider is the Reynolds number R_e. This dimensionless parameter is defined as follows [11]:

$$R_e = \frac{\rho \bar{c} V_a}{\mu} = \frac{\bar{c} V_a}{\nu} , \quad (17)$$

where a characteristic length of the system is $\bar{c}$ chosen to be the wing mean chord, the airspeed is V_a, the air density is ρ, the air dynamic viscosity is μ, and the air kinematic viscosity is ν as defined in the Appendix. With a speed range from $[0 \ldots 20]$ m/s, and a characteristic length (mean wing chord $\bar{c} = 0.2$ m), the Reynolds number for this plane is within the range of $R_e = [0 \ldots 260000]$ approximatively.

With the knowledge of the Reynolds number and the type of wing profile (in this case, the *Clark Y profile*), it is possible to check on recorded data the corresponding curves for the lift, drag and moment coefficients as a function of the angle of attack. Figures 3 and 4 shows the dimensionless lift and drag coefficients C_Z and C_D as a function of the angle of attack. These plots have been obtained based on data generated by XFoil [1] for different Reynolds numbers and a Crit number $N_{Crit} = 9$ corresponding to nominal turbulence conditions of a wind tunnel.

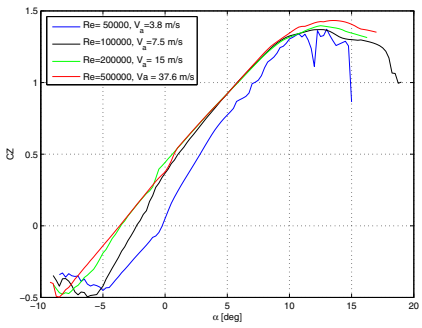

Fig. 3. Dimensionless lift coefficient C_Z as a function of α

The wing dimensionless lift and drag coefficients: C_Z and C_D, can be approximated by two sets of functions. The first set is used up to the stall angle of attack α_{s+} (resp. α_{s-}) for positive (resp. negative) angle of attack, and the second set for the post-stall region.

In the pre-stall region, the wing aerodynamic coefficients are modeled by [10]

$$\begin{aligned} C_{Z,l}(\alpha, V_a) &= C_{Z,0}(V_a) + C_{Z,\alpha}(V_a)\alpha \,, \\ C_{D,l}(\alpha) &= C_{D,0}(V_a) + C_{D,\alpha}(V_a)\alpha^2 \,. \end{aligned} \quad (18)$$

In the post stall region, the wing lift and drag coefficients are modeled as [8]

$$\begin{aligned} C_{Z,s}(\alpha) &= c_1 \sin(2\alpha) \,, \\ C_{D,s}(\alpha) &= c_0 + 2c_1 \sin^2(\alpha) \,. \end{aligned} \quad (19)$$

with the constant terms c_0 and c_1. Remarks:

- We note that lift data are mostly independent of the Reynolds number when the angle of attack is beyond the stall angle $\alpha_{s\pm}$.
- For small angle of attack and small Reynolds number up to $R_e = 10^5$, the offset lift $C_{Z,0}$ is increasing as a function of the airspeed, whereas the slope $C_{Z,\alpha}$ decreases as the speed increases, up until an asymptotic value $\overline{C}_{Z,\alpha}$, see Table I.

The pre-stall and post-stall regions described by Eqs. (18) and (19) can be blended (as proposed by [8]) using a pseudo-sigmoid function $\sigma(\alpha_+, \alpha_-, \alpha)$ defined by [8]

$$\sigma(\alpha_+, \alpha_-, \alpha) = \begin{cases} \frac{1+\tanh(k_+(\alpha_+^2 - \alpha^2))}{1+\tanh(k_+\alpha_+^2)}, & \alpha \in [0, \pi/2] \\ \frac{1+\tanh(k_-(\alpha_-^2 - \alpha^2))}{1+\tanh(k_-\alpha_-^2)}, & \alpha \in [-\pi/2, 0) \end{cases}$$

where the parameters α_+ and α_- correspond to the switching point of the pseudo-sigmoid function, and can be chosen around the stall angles α_{s+} for positive angle α and α_{s-} for

[1] http://airfoiltools.com/airfoil/

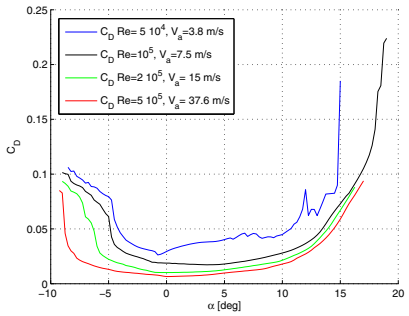

Fig. 4. Dimensionless lift coefficient C_D as a function of α

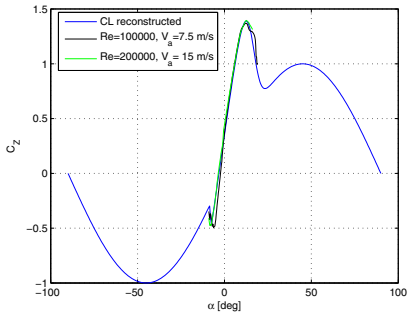

Fig. 5. Wing lift dimensionless coefficient C_Z: reconstructed superposed with C_Z from XFoil data for $Re = \{10^5,\ 2\,10^5\}$

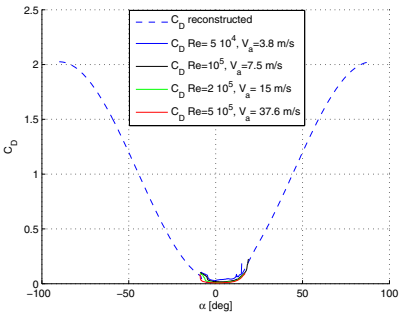

Fig. 6. Wing drag dimensionless coefficient C_D: reconstructed superposed with C_D from XFoil data.

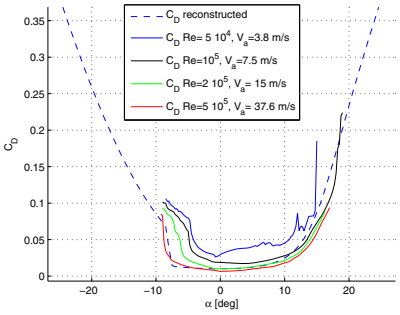

Fig. 7. (Zoom) Wing drag dimensionless coefficient C_D: reconstructed superposed with C_D from XFoil data.

negative angle α, whereas the parameter k_+ and k_- set the rate of transition and should be chosen larger than 1.

$$C_Z(\alpha) = \sigma_{(\alpha_+,\alpha_-,\alpha)} C_{Z,l}(\alpha, V_a) + (1 - \sigma_{(\alpha_+,\alpha_-,\alpha))} C_{Z,s}$$
$$C_D(\alpha) = \sigma_{(\alpha_+,\alpha_-,\alpha)} C_{D,l}(\alpha, V_a) + (1 - \sigma_{(\alpha_+,\alpha_-,\alpha))} C_{D,s}$$

Figures 5 and 6 (and 7) show the construction of the lift and drag coefficients C_Z and C_D over a large range of angle of attack and compared to the data provided by XFoil for $Re = \{10^5,\ 2\,10^5\}$ using

$$\alpha_+ = \frac{15\pi}{180}, \alpha_- = \frac{9\pi}{180}, k_+ = 20, k_- = 800,$$
$$C_{Z,0} = 0.35, C_{Z,\alpha} = 0.11, C_{D,0} = 0.01, C_{D,\alpha} = 0.2,$$
$$c_1 = 1, c_0 = 0.025.$$

C. Lift Force

The lift force is calculated by multiplying the lift coefficient by the wing surface S and the dynamic pressure $\bar{q}$ as: $Z^{\mathcal{W}} = \bar{q} S C_Z(\alpha)$.[2] The lift and drag forces of the wing are typically applied at a point located at 25% distance from the front-edge of the wing, and is known as the aerodynamic center.

D. Lateral Force

The lateral force acting on the aircraft is mainly due to the fuselage, which is considered to be an inefficient wing with zero offset due to the symmetry of the airplane in the (x_b, z_b) plane, yielding (we consider that the sideslip angle β remains rather small, *i.e.* within the range $[-20, +20]$)

$$C_Y(\beta) = C_{Y1}\beta\ , \qquad Y^{\mathcal{W}} = \bar{q} S C_Y(\beta)\ . \tag{20}$$

E. Drag Force

Due to the symmetry of the fuselage, minimum drag is obtained when the sideslip angle β is zero. The wing is not symmetric, therefore, minimum drag is obtained for an angle of attack different from zero. The dimensionless drag coefficient is approximated by a quadratic function in α and β according to $C_X(\alpha, \beta) = C_D(\alpha) + C_{X\beta 2}\beta^2$. The drag force is obtained as $X^{\mathcal{W}} = \bar{q} S C_X(\alpha, \beta)$.

Remark: Each wing can be divided into two parts (one piece along y_b and one piece for the swept part), and the above modeling can be applied to each part, creating a total force and moment due to the wing.

V. AERODYNAMICS MOMENTS

The torques are denoted $[L \quad M \quad N]^T$ on each body axis respectively. They are generated by control surfaces such as ailerons, elevators, and rudders. The control surface deflections are scaled such that the range of δ_a, δ_e, and δ_r are the same: $\delta_a, \delta_e, \delta_r \in [-1, 1]$. The total torque $\mathbf{\Gamma}_a$ applied to the airframe containing only aerodynamics effects and is expressed in the body-fixed frame as $\mathbf{\Gamma}_a^{\mathcal{B}} = \begin{bmatrix} L^{\mathcal{B}} & M^{\mathcal{B}} & N^{\mathcal{B}} \end{bmatrix}^T$.

[2]The superscript $\mathcal{W}$ indicates that the vector is expressed in the wind frame.

A. Roll Torque $L^{\mathcal{B}}$

The generation of the roll torque is modeled by a linear function of the aileron deflection δ_a, the sideslip angle β, and the dimensionless angular rates $\tilde{p}$ and $\tilde{r}$. The dimensionless angular rates are $\tilde{p} = \frac{bp}{2V_a}$, $\tilde{q} = \frac{\bar{c}q}{2V_a}$, $\tilde{r} = \frac{br}{2V_a}$, where the wingspan is b and the mean aerodynamic chord is $\bar{c}$. The dimensionless roll torque is

$$C_L(\delta_a, \beta, \tilde{p}, \tilde{r}) = C_{La}\delta_a + C_{L\beta}\beta + C_{L\tilde{p}}\tilde{p} + C_{L\tilde{r}}\tilde{r} \ . \quad (21)$$

The effectiveness of the ailerons to produce some roll torque is modeled through the coefficient C_{La} and depends mainly on the size of the ailerons. The term $C_{L\tilde{p}}$ is the damping factor related to the dimensionless roll rate $\tilde{p}$. The term $C_{L\tilde{r}}$ is useful to model the effect of unequal left and right wing speeds due to the rotation around the z_b axis, resulting in a difference in the lift forces, and thus modifying the roll torque generation. The roll torque is then obtained by multiplying $C_L(\delta_a, \beta, \tilde{p}, \tilde{r})$ by the dynamic pressure $\bar{q}$ and the wing surface S as $L^{\mathcal{B}} = \bar{q}SbC_L(\delta_a, \beta, \tilde{p}, \tilde{r})$.

B. Pitch Torque $M^{\mathcal{B}}$

The generation of the pitch torque $M^{\mathcal{B}}$ expressed in the aircraft body-fixed frame (b) is modeled by a linear function of the elevator deflection δ_e, of the angle of attack α, and of the dimensionless pitch rate $\tilde{q}$. The dimensionless pitch torque is modeled as

$$C_M(\delta_e, \alpha, \tilde{q}) = C_{M1} + C_{M_e}\delta_e + C_{M\tilde{q}}\tilde{q} + C_{M\alpha}\alpha \ . \quad (22)$$

The effectiveness of the elevator to produce some pitch torque is accounted for through the coefficient C_{Me} and is dependent mainly on the size of the elevator. The derivative term $C_{M\alpha}$ is negative if the airplane is stable on its longitudinal axis. The damping factor $C_{M\tilde{q}}$ depends mainly on the length of the fuselage and the surface of the horizontal tail. The pitch torque is finally $M^{\mathcal{B}} = \bar{q}S\bar{c}C_M(\delta_e, \alpha, \tilde{q})$.

C. Yaw Torque $N^{\mathcal{B}}$

The generation of the yaw torque $N^{\mathcal{B}}$ is modeled by a linear function of the rudder deflection δ_r, of the sideslip angle β, and of the dimensionless yaw rate $\tilde{r}$ as follows:

$$\begin{aligned} C_N(\delta_r, \tilde{r}, \beta) &= C_{N_{\delta_r}}\delta_r + C_{N\tilde{r}}\tilde{r} + C_{N\beta}\beta \ , \\ N^{\mathcal{B}} &= \bar{q}SbC_N(\delta_r, \tilde{r}, \beta) \ . \end{aligned} \quad (23)$$

The effectiveness of the rudder to produce some yaw torque is modeled through the coefficient $C_{N_{\delta r}}$ and is dependent mainly on the size of the rudder. The damping factor $C_{N\tilde{r}}$ is affected by primarily the lever arm and the size of the vertical tail.

VI. CONCLUSIONS

This paper describes a novel type of flying machine, which combines the four rotor of a quadrotor and the wing and fuselage of a conventional fixed-wing airplane. The orientation of the propellers can be changed thanks to a tilting mechanism. The paper aims at modeling the major forces and moments acting on the hybrid vehicle, also at high angle of attack. This model serves as a basis for a simulator, to first test and validate flight controllers on such a convertible vehicle.

REFERENCES

[1] E. Cetinsoy, S. Dikyar, C. Hancer, K.T. Oner, E. Sirimoglu, M. Unel, and M.F. Aksit. Design and construction of a novel quad tilt-wing UAV. *Mechatronics*, 22(6):723–745, 2012.

[2] M.-D. Hua, T. Hamel, and C. Samson. Control of VTOL vehicles with thrust-tilting augmentation. In *19th IFAC World Congress*, 2014.

[3] Y. Long and D.J. Cappelleri. Linear control design, allocation, and implementation for the omnicopter MAV. In *IEEE International Conference on Robotics and Automation*, pages 289–294, 2013.

[4] S. Newman. *The foundations of helicopter flight*. Halsted Press, 2001.

[5] K. T. Oner, E. Cetinsoy, M. Unel, M. F. Aksit, I. Kandemir, and K. Gulez. Dynamic model and control of a new quadrotor unmanned aerial vehicle with tilt-wing mechanism. *International Journal of Applied Science, Engineering & Technology*, 5(2), 2009.

[6] C. Papachristos, K. Alexis, and A. Tzes. Design and experimental attitude control of an unmanned tilt-rotor aerial vehicle. In *IEEE International Conference on Advanced Robotics*, pages 465–470, 2011.

[7] D.K. Phung and P. Morin. Modeling and energy evaluation of small convertible UAVs. In *2nd Workshop on Research, Education and Development of Unmanned Aerial Systems*, 2013.

[8] Daniele Pucci, Tarek Hamel, Pascal Morin, and Claude Samson. Nonlinear control of aerial vehicles subjected to aerodynamic forces. In *IEEE Conf. on Decision and Control*, 2013.

[9] M. Ryll, H.H. Bulthoff, and P.R. Giordano. First Flight Tests for a Quadrotor UAV with Tilting Propellers. In *IEEE International Conference on Robotics and Automation*, pages 295–302, 2013.

[10] R. F. Stengel. *Flight Dynamics*. Princeton University Press, Princeton, New Jersey, 2004.

[11] B. Stevens and F. Lewis. *Aircraft Control and Simulation, Second Edition*. Wiley, New York, NY, 2003.

[12] D.A. Ta, I. Fantoni, and R. Lozano. Modeling and control of a convertible mini-UAV. In *Proceedings of the 18th IFAC World Congress*, pages 1492–1497, 2011.

APPENDIX

TABLE I

SOME PHYSICAL PARAMETERS OF THE AIRCRAFT

Weight m	2.7 [kg]
Wingspan b	2 [m]
wing mean chord $\overline{c}$	0.2 [m]
Length L	1.16 [m]
Maximum thrust per rotor	1 [kg]
Propeller type	APC MR 10x5.5
Max propeller speed	8700 [rpm]
CoM location	11 cm from the front edge of the wing
$L_0, \quad l_0$	0.29 [m], 0.215 [m]
$l_1 \quad h_1$	0.16 [m], 0.05 [m]
air viscosity μ $(18°C)$	18.27 10^{-6}[Pa s]
air density $(18°C)$ ρ	= 1.2150 [kg/m^3]
$C_{Z,0} \quad (Re \geq 10^5)$	0.35
$\overline{C}_{Z,\alpha}$	0.11
$C_{D,0} \quad C_{D,\alpha}$	0.01 0.2
positive stall angle of attack: α_{s+}, $R_e = \{5.10^4, 10^5, 2.10^5, 5.10^5\}$	$\{12.5, 13, 13.5, 13.5\}$ deg
negative stall angle of attack: α_{s-}, $R_e = \{5.10^4, 10^5, 2.10^5, 5.10^5\}$	$\{-5, -6, -8, -8.5\}$ deg
$c_0 \quad c_1$	0.025 1